Int. J. Multiphase Flow, Vol. 4, pp. 461–486. Pergamon/Elsevier, 1978. Printed in Great Britain

FLOW STRUCTURE AND DISTRIBUTION EFFECTS IN GAS–LIQUID MIXTURE FLOWS

R. A. HERRINGE
M.D. Research Company Pty Limited, P.O. Box 22, North Ryde, N.S.W. 2113, Australia

and

M. R. DAVIS
School of Mechanical and Industrial Engineering, University of New South Wales, Kensington, N.S.W. Australia

(*Received* 1 *September* 1977)

Abstract—Air–water mixtures which are assumed to flow homogeneously in a pipe are usually described by a one-dimensional momentum balance. This allows definition of a friction factor in a manner similar to single phase flows. By defining a momentum flux distribution parameter, the momentum balance has been modified to correctly include the effects of phase and velocity distributions and the effect of these on calculated friction factors has been investigated. Resistivity probes were used to measure void fraction and gas phase velocity distributions for selected vertical and horizontal flow conditions, and these were combined with static pressure measurements to calculate friction factors. For bubbly flows, the inclusion of these distribution effects did not substantially alter friction factor estimates which are approximately 10% above single phase values (for Reynolds numbers based on liquid viscosity).

Friction factor values are shown to be related to flow development with higher values associated with developing flows. In particular, high friction factors are associated with the need to break-up bubbles to an "equilibrium" size. In order to experimentally simulate fully developed vertical flows, the highly turbulent nozzle mixer is most suitable while the less turbulent wall-injection type seems appropriate for horizontal flows.

INTRODUCTION

For the flow of gas–liquid mixtures through pipes, there are three factors which contribute to the overall pressure drop: wall friction, gravity, and acceleration due to expansion of the gas phase. Attempts to correlate the frictional pressure losses are complicated by the difficulties of isolating this particular component since determination of the other two components requires some knowledge of velocity and density distributions across the flow. The simplest approach is to restrict discussion to the case of homogeneous, or well-mixed, flows in which phase and velocity distribution effects are neglected. This allows estimates of gravitational and acceleration components of pressure drop to be based on local volumetric flow ratios, calculated by knowledge of the mass flows and local static pressure, and by regarding the flow as a compressible fluid mixture. This approach has been adopted by several authors including Huey & Bryant (1967), Kopalinsky & Bryant (1976), Rose & Griffith (1964) and by Davis (1974). In each of these studies, the authors used a compressible flow momentum balance (to be combined with static pressure data) in order to determine a wall friction factor, defined on the basis of an average mixture velocity and density, similar to single phase flows. However, for Reynolds numbers (based on liquid viscosity) below 10^5, Wallis (1969) suggests that experimental friction factors are scattered with no clear trends evident, so that a constant value of 0.005 was recommended. Davis (1974) considered flows with Reynolds numbers above 10^5 and found that friction factors were in general about 10% above the equivalent single phase values. All of the data points considered by Davis were within 5% of a mean curve drawn through the data, provided the void fraction was not too high. The maximum limit of void fraction for the observed correlation was described in terms of a sonic point void fraction, α^* such that $\alpha^* < 0.85$. For higher void fractions, slightly lower values of friction factor were computed. Davis suggested that the modification to the frictional behaviour at high void fractions may be caused by some substantial overall separation between the phases within the flow, even though this was not directly apparent by external visual observations. Whether there is a true change in

friction factor or only an apparent change caused by errors in the momentum balance due to distribution effects is uncertain without investigating the flow structure in detail. Similarly, Kopalinsky & Bryant (1976) who experimented at high Reynolds numbers for nominally homogeneous flow reported that friction factors varied significantly at higher values of void fraction. In a similar manner to Davis, their results showed an initial increase in friction factor with gas content (represented by a mass flow ratio in this case), followed by a decrease in friction factor for higher gas content. Beattie (1973) calculated friction factors based on a homogeneous treatment and showed that with suitable definition of the Reynolds number, bubble flow friction factors were essentially equivalent to single-phase values.

Together with data from various other sources Beattie demonstrated the correlation using data from Kopalinsky (1971) which has been subsequently published by Kopalinsky & Bryant (1976). However, while Beattie's correlation shows generally satisfactory overall agreement with the data it does not account for the decrease in friction factor for high gas content.

In this paper, the analytical approach adopted by Davis has been extended to allow for velocity and concentration distributions in the form of a velocity ratio and a momentum flux distribution parameter. When combined with experimental static pressure measurements, the analysis allows calculation of friction factors which can be compared with values from the homogeneous flow model. The pressure drop experiments were carried out simultaneously with measurements of the flow structure which gave values of the local gas content in terms of the void fraction, as well as other parameters including estimates of bubble diameters and velocity distributions. In addition, the methods for the study of internal flow structure described by Herringe & Davis (1976) are applied here in more detail and extended to the study of both horizontal and vertical pipe flows.

ONE-DIMENSIONAL MOMENTUM BALANCE

The flow of a two-phase mixture along a circular pipe may be analysed by considering the equilibrium of wall shear stress, gravitational forces, momentum changes and the static pressure gradient. The force balance equation is

$$-\frac{dp}{dx} = \frac{4}{d}\tau_w + \rho_m g \frac{d}{4}\sin\theta + \frac{d}{dx}<\alpha\rho_G u_G^2 + (1-\alpha)\rho_L u_L^2>, \qquad [1]$$

where: x = axial position; p = static pressure; g = gravitational acceleration; u = local velocity; α = void fraction; ρ = density; τ_w = wall shear stress, and θ = angle of inclination to horizontal. Subscripts: L = liquid, G = gas; and the operator $\langle\ \rangle$ denotes area average values

$$\rho_m = \langle\alpha\rangle\rho_G + \langle 1-\alpha\rangle\rho_L. \qquad [2]$$

The prediction of the pressure gradient requires some means of estimating the three terms on the right hand side of [1]. Generally, the first term is evaluated with the aid of an empirical friction factor and the second and third terms are approximated, assuming a homogeneous flow model or by allowing for relative phase velocities and approximating the third term. The approximate equation based on the homogeneous flow model is

$$-\frac{dp}{dx} = \frac{4}{d}\tau_w + \rho g \frac{d}{4}\sin\theta + \frac{d}{dx}(\rho u^2), \qquad [3]$$

where $\rho = \beta\rho_G + (1-\beta)\rho_L$ and β = gas volume flow/total volume flow,

$$= Q_G/(Q_G + Q_L),$$

$$u = (Q_G + Q_L)/(\pi d^2/4),$$

and the approximate equation which allows for separate phase velocities is (Herringe 1973)

$$-\frac{dp}{dx} = \frac{4}{d}\tau_w + \rho_m g \frac{d}{4}\sin\theta + \frac{d}{dx}(\langle\alpha\rangle \rho_G \bar{u}_G^2 + \langle 1-\alpha\rangle \rho_L \bar{u}_L^2), \quad [4]$$

where,

$$\bar{u}_G = \frac{\langle \alpha u_G\rangle}{\langle\alpha\rangle} \quad [5]$$

and,

$$\bar{u}_L = \frac{\langle (1-\alpha) u_L\rangle}{\langle 1-\alpha\rangle} \quad [6]$$

As pointed out by Beattie (1973), neither of these approximations is strictly correct, but the terms are more easily evaluated than the terms in [1]. Usually, the wall shear stress is determined by experimentally measuring the pressure gradient and evaluating the second and third terms. A friction factor is then introduced with a definition similar to

$$f = \tau_w \Big/ \left(\frac{1}{2}\rho u^2\right). \quad [7]$$

By using [7] (or a similar definition) with either [3] or [4] a friction factor (more accurately termed a loss coefficient for these two cases) can be evaluated, and as discussed previously these loss coefficients have been empirically related to a suitably defined Reynolds number. However, if the terms of [1] can be accurately determined then the frictional term can be correctly isolated from the other components of the pressure gradient and a true friction factor determined.

The analysis which follows provides a means of explicitly integrating [1] along the pipe, with none of the assumptions of the homogeneous model or the alternative approach allowing for separate phase velocities. However, the analysis does require empirical friction factors and empirical means of predicting the void fraction and momentum at inlet to the pipe. The analysis is subsequently used in conjunction with experimental data to evaluate these parameters.

To assist with the analysis, a momentum flux distribution parameter is introduced, defined by

$$K = \frac{\langle \alpha \rho_G u_G^2 + (1-\alpha)\rho_L u_L^2\rangle}{\langle\alpha\rangle \rho_G \bar{u}_G^2 + \langle 1-\alpha\rangle \rho_L \bar{u}_L^2}, \quad [8]$$

and the velocity ratio is defined by

$$S = \bar{u}_G / \bar{u}_L. \quad [9]$$

The continuity equation for each phase is

$$\frac{d}{dx}\langle \alpha \rho_G u_G\rangle = 0, \quad [10]$$

and

$$\frac{d}{dx}\langle (1-\alpha)\rho_L u_L\rangle = 0, \quad [11]$$

which gives, using [5] and [6] and the assumption that the gas phase density is constant across the section

$$\frac{d}{dx}(\langle\alpha\rangle\rho_G\bar{u}_G) = 0, \quad [12]$$

and

$$\frac{d}{dx}(\langle 1-\alpha\rangle\rho_L\bar{u}_L) = 0. \quad [13]$$

Combining [8], [9], [12] and [13] with [1] gives

$$-\frac{dp}{dx} = \frac{4}{d}\tau_w + \rho_m g\frac{d}{4}\sin\theta + \frac{\langle\alpha\rangle}{\rho_G}\frac{d\rho_G}{dx}\cdot(\rho u^2)_m + \frac{(\rho u^2)_m}{K}\frac{dK}{dx} + \frac{\langle\alpha\rangle\langle 1-\alpha\rangle}{S}K\frac{dS}{dx}\cdot(\rho_L\bar{u}_L^2 - \rho_G\bar{u}_G^2) \quad [14]$$

where $(\rho u^2)_m$ = momentum of mixture

$$= \langle\alpha\rho_G u_G^2 + (1-\alpha)\rho_L u_L^2\rangle. \quad [15]$$

For polytropic expansion of the gas phase, (P/ρ_G^n) = constant, which can be substituted into [14] to give

$$\frac{dp}{dx}(1-\langle\alpha\rangle D/n) + \frac{2f}{d}\cdot D_\rho + \rho_m g\frac{d}{4}\sin\theta + T_1 + T_2 = 0, \quad [16]$$

where:

$$D = (\rho u^2)_m/p;$$

$$T_1 = \frac{(\rho u^2)_m}{K}\frac{dK}{dx},$$

and

$$T_2 = \langle\alpha\rangle\langle 1-\alpha\rangle\frac{K}{S}\frac{dS}{dx}(\rho_L\bar{u}_L^2 - \rho_G\bar{u}_G^2),$$

and the friction factor f is defined by

$$\tau_w = f.\frac{1}{2}(\rho u^2)_m. \quad [17]$$

It is likely that T_1 and T_2 will be negligible for fully developed flow situations (where entrance effects are negligible), so that with this assumption

$$\frac{dp}{dx}(1-\langle\alpha\rangle D/n) + \frac{2f}{d}Dp + \rho_m g\frac{d}{4}\sin\theta = 0, \quad [18]$$

$$\frac{d\bar{p}}{d\xi}(1-\langle\alpha\rangle D/n) + 2D\bar{p} + \frac{D}{fF}\bar{p}\sin\theta = 0, \quad [19]$$

where

$$\xi = \frac{fx}{d}, \quad F = \frac{(\rho u^2)_m}{\rho_m g d} \quad \text{and} \quad \bar{p} = \frac{p}{p_o},$$

and the subscript zero denotes conditions at the reference point $x = 0$.

By introducing the equations of state from the appendix, and assuming a developed flow so that $K = K_0$ and $S = S_0$, [19] may be rearranged in the form

$$\frac{d\bar{p}}{d\xi}\left\{1 - \frac{\langle\alpha_0\rangle D_0}{n}\bar{p}^{-(1/n+1)}\right\} + 2D_0\{1 - \langle\alpha_0\rangle + \langle\alpha_0\rangle\bar{p}^{-1/n}\} + \frac{D_0}{F_0 f}\cdot\frac{1}{1 - \langle\alpha_0\rangle + \langle\alpha_0\rangle\bar{p}^{-1/n}}\sin\theta = 0. \quad [20]$$

The pressure distribution $\bar{p}(\xi)$ along the pipe follows directly from [20] and the form depends on the inlet values of void fraction $\langle\alpha_0\rangle$, dynamic head factor D_0, index of compression of the gas phase n and the product of friction factor and Froude number, $f F_0$.

Equation [20] is identical to the expression developed by Davis (1974) for homogeneous flows. The difference in the use of the equations is that values of $\langle\alpha\rangle$, D and F should be determined from the true in-line void fraction and momentum rather than from the homogeneous approximations. Davis further developed [20] and showed that for horizontal flow the pressure distribution can be expressed in terms of a single parameter: the void fraction at the sonic point. In order to carry out a similar analysis, it is necessary to define the Mach number of the flow. An expression for the speed of sound for the mixture is derived in the appendix as

$$a = \sqrt{\left(\frac{n_i p}{\langle\alpha\rangle\rho_m}\right)}, \quad [21]$$

where n_i is the compression index of the gas phase which allows isotropic compression of the mixture.

The Mach number is given by

$$M = u/a, \quad [22]$$

where u is some characteristic velocity of the flow, which must be defined to be consistent with other flow parameters. Such a definition for u is given by

$$u^2 = (\rho u^2)_m/\rho_m, \quad [23]$$

which gives the Mach number as

$$M = \sqrt{(\langle\alpha\rangle D/n_i)}. \quad [24]$$

The condition for choked flow ($d\xi/d\bar{p} = 0$) is

$$\sqrt{(\langle\alpha\rangle D/n)} = 1,$$

so that the Mach number which corresponds to choking is

$$Mc = \sqrt{(n/n_i)}.$$

It is reasonable to assume that the gas phase expands isothermally, so that $n = 1$, giving

$$Mc = \sqrt{(1/n_i)},$$

and as discussed in the appendix $n_i \approx 1$, so that $Mc \approx 1$.

If the critical, or sonic, conditions are denoted by an asterisk then, since $M^* = 1$,

$$D^* = 1.$$

The pressure is now normalized on the basis of the pressure at the sonic point, putting $\bar{p}^* = p/p^*$, and [20] for the horizontal flow case can be integrated to give

$$\xi^* = \frac{(1-\bar{p}^*)}{2(1/\langle\alpha^*\rangle - 1)} - \frac{1}{2}\ln\left\{\frac{1-\langle\alpha^*\rangle + \langle\alpha^*\rangle\bar{p}^{*-1}}{((1-\alpha^*)\bar{p}^* + \langle\alpha^*\rangle)^{\langle\alpha^*\rangle/(1-\alpha^*)^2}}\right\}. \quad [25]$$

This equation expresses the pressure distribution $\bar{p}^*(\xi^*)$ only in terms of the void fraction at the sonic point $\langle\alpha^*\rangle$, which can be evaluated from (as shown by Davis)

$$\langle\alpha^*\rangle = \frac{1}{1-\langle\alpha_0\rangle\sqrt{(D_0/\langle\alpha_0\rangle)+1}}. \quad [26]$$

DISTRIBUTION EFFECTS AND FRICTION FACTORS

The friction factor defined by [17] can be evaluated from [16] and static pressure measurements provided there is sufficient experimental information available to evaluate $\langle\alpha\rangle$, D, T_1 and T_2. If the shapes of the velocity and concentration distributions do not change then K and S are constant, so that T_1 and T_2 are zero. It is then necessary to determine $\langle\alpha\rangle$ and D. The homogeneous flow model [3], uses approximations for both $\langle\alpha\rangle$ and D and the effect of these approximations on the calculated friction factor can be seen by considering small errors in $\langle\alpha\rangle$ or D. If $\langle\alpha\rangle$ and D are considered for the moment as independent variables, then for horizontal flows, [18] gives the following expression for errors in calculated friction factors due to using incorrect values of $\langle\alpha\rangle$ and D.

$$\frac{df}{f} = \frac{-\langle\alpha\rangle D/n}{(1-\langle\alpha\rangle D/n)}\cdot\frac{d\langle\alpha\rangle}{\langle\alpha\rangle} - \frac{1}{1-\langle\alpha\rangle D/n}\cdot\frac{dD}{D}. \quad [27]$$

These errors can be evaluated if the shape of void fraction and velocity profiles are known. Beattie (1972) compared with the profile shapes of various flow models with experimental data, and for bubble flows having only a single maximum in their void profiles, he proposed a "voidage deficiency" equation of the form

$$(1-\alpha)^{3/2} = (1-\alpha_c)^{3/2} - 3u^*a/2k\ln(y/y_c) \quad [28]$$

where: y = distance from wall; y_c = distance to maximum α; k = mixing length constant; $u^* = \sqrt{(\tau_w/\rho_L)}$; a = constant defined by $\alpha = au_L + b$; u_L = liquid velocity; b = constant defined above; and for velocity profiles he combined [28] with

$$\alpha = au_L + b \text{ and } \alpha = cu_G + d \quad [29]$$

where C and d are constants. Beattie compared these relations with experimental data and alternative shapes proposed elsewhere. For bubble flow the relations generally fitted data better than the forms proposed by Zuber *et al.* (1967)

$$\alpha/\alpha_c = 1-(r/R)^n, \quad [30]$$

$$u/u_c = 1-(r/R)^m, \quad [31]$$

where r = distance from centre, u_c = velocity at centre, R = pipe radius, and "as well, or better than" the forms proposed in Bankoff's variable density model

$$\alpha/\alpha_c = (y/R)^{1/n}, \quad [32]$$

$$u/u_c = (y/R)^{1/m}, \quad [33]$$

where u and u_c refer to either the gas or liquid phase.

Although [28] and [29] provide a marginally better fit to available data than do [32] and [33], the latter pair will be used in the following analysis for simplicity in demonstrating distribution effects.

The homogeneous flow model uses the volumetric flow ratio, β instead of $\langle\alpha\rangle$, where

$$\beta = \frac{\langle \alpha u_G \rangle}{\langle \alpha u_G + (1-\alpha) u_L \rangle}. \qquad [34]$$

For distributions described by [32] and [33], β will be greater than $\langle\alpha\rangle$ if m and n are positive. For example, consider the simplest case with the assumption $u = u_G = u_L$, then

$$\beta = \langle \alpha u \rangle / \langle u \rangle,$$

and by evaluating the area averages by integration gives

$$\beta = \langle \alpha \rangle \cdot \frac{(1+n)(1+m)(1+2n)(1+2m)}{2(m+n+mn)(m+n+2mn)}, \qquad [35]$$

so that $\beta > \langle\alpha\rangle$ for all positive values of m and n.

Similarly, the homogeneous flow model used, for D

$$D_h = \rho u^2 / p,$$

i.e.

$$D_h = (\beta\rho_G + (1-\beta)\rho_L)\langle \alpha u_G + (1-\alpha)u_L \rangle^2 / p, \qquad [36]$$

and an expression similar to [35] (although a much longer algebraic expression) related D_h and D. In general, for typical values of m and n, $D_h < D$ and typically $|dD| = |Dh - D|$ is less than $0.04D$. For example, with $\alpha_m = 0.5$, $m > 5$ and $n < 50$, then $|dD/D| < 0.035$. Hence, on the basis of the variable density model approach we would expect that the first term on the right of [27] would contribute a negative error in f while the second term contributes a positive error, and the relative values of these contributions will depend on the actual flow distributions and on the magnitude of the product $\langle\alpha\rangle D$. In most cases of bubble or dispersed flow, $\langle\alpha\rangle D \ll 1$, so that the second term of [27] will dominate, leading to overestimates of friction factors when the analysis is based on the homogeneous model.

If the momentum balance by [4] is used then the only error in friction factor results from dD/D, since correct values of void fraction are used. In this case,

$$dD/D = (1-K)/K, \qquad [37]$$

where K is defined in [8]. K can be evaluated as a function of m, n, α_c and u_c for the gas and liquid phases with the result that $K > 1$ and approaches 1 as m becomes very large. Hence, even if allowance is made for the relative phase velocities, the value of D will be underestimated, leading to an overestimate in the friction factor. Further, it can also be shown using the variable density approach that the error in D is likely to be greater when the relative phase velocity model is used than when the homogeneous model is used. Although it was stated above that $D_h < D$ in general, D_h can equal D and for extreme cases ($m > 20$ say) D_h can be greater than D (although less than 1% greater).

Overall, it is likely that for most horizontal conditions, the homogeneous flow model would give values of friction factor closer to the true values than values given by the relative phase velocity model. This results from the expected lower values of dD/D for the homogeneous

model, and the compensating effect of the $d\langle\alpha\rangle/\langle\alpha\rangle$ term. It is only for extreme cases when the $d\langle\alpha\rangle/\langle\alpha\rangle$ term might dominate that the homogeneous model would be expected to introduce significant errors.

For vertical flows, the homogeneous flow model includes an additional error due to the use of the incorrect density in calculating the static head term. If [17] is rearranged to be explicit in f, then the static head term is proportional to $\rho_m/(\rho u^2)_m$. The homogeneous model underestimates both ρ_m and $(\rho u^2)_m$ so that these errors tend to compensate one another.

EXPERIMENTAL MEASUREMENTS

To determine the magnitude of distribution effects, local values of void fraction and phase velocities are required. To determine these, needle resistivity probes were used, as described in more detail by Herringe & Davis (1974). Basically, the probes consist of a needle pointing into the flow, electrically insulated everywhere except at the tip. The electrical resistance between the tip and an earth electrode is measured and indicates whether there is air or water surrounding the tip. The average time that the probe is in air is an indication of the local void fraction and by traversing a probe across a section, the void fraction distribution can be measured. The area average void fraction can then be determined by averaging the profiles across the pipe section.

By locating two probes, displaced in the flow direction a distance Δx and correlating the signals to determine the time delay which gives maximum correlation Δt the convection velocity of the discontinuous phase can be determined by

$$u = \Delta x/\Delta t.$$

In the case of bubble flows, this gives the local gas phase velocity, u_G. Using the resistivity probe technique, there is no means of measuring local velocities of the liquid phase, although realistic assumptions can be made, as will be subsequently discussed.

The reliability of this technique can be gauged by calculating the gas volume flux from the void and velocity profiles, and comparing these with values calculated from flow rate and static pressure measurements. This was done by Herringe & Davis (1976) for the vertical flow conditions discussed in this paper with the result that the average deviation of the two quantities was less than 6%, with the integrated average values tending to be low, probably due to deflection of small bubbles. The details of the resistivity probe calibration techniques are fully explained by Herringe & Davis (1974).

Bubble size measurements can also be made with the needle probes. The diameter of each detected bubble is determined from its detected chord length which is defined as the product of the mean bubble velocity and the period during which the probe is in the gas phase. By suitable signal conditioning, and with the aid of a Correlator/Probability Analyser, frequency distributions of bubble diameters were obtained. This involved several assumptions, the most important being that all bubbles are spherical and travel with the convection velocity u_c. The mean diameter of detected bubbles results immediately from the frequency distributions, and this is the value which will be referred to in subsequent discussion. However, it should be noted that the frequency distribution of detected bubbles is not necessarily representative of the total bubble population since there is a greater likelihood of detecting larger bubbles. This aspect is discussed in more detail together with the more complete analysis and signal interpretations by Herringe & Davis (1976).

Pressure measurements were made by use of mercury manometers, with a needle valve to dampen fluctuations to within $\pm 2\%$. Air and water flow rates were measured with orifice plates, constructed to British Standard BS 1042 and for both fluids, two sizes were used to allow a wide range of flow conditions to be measured.

Table 1. Flow rates for standard flow conditions. Reynolds number is based on mixture velocity and density and liquid phase viscosity

Flow condition	Air flow rate ($kg/s \times 10^3$)	Water flow rate (kg/s)	Superficial velocities at 36D (m/s) Water	Air	Reynolds number *Re*	Froude number *Fr*
1	0.57	3.80	1.88	0.18	0.92	9.0
2	1.27	3.80	1.88	0.41	0.92	11.6
3	2.68	3.80	1.88	0.87	0.92	17.5
4	2.68	8.46	4.19	0.76	2.05	51.0
5	3.44	8.46	4.19	0.86	2.05	54.8
6	10.45	8.46	4.19	2.36	2.05	92.0
7	4.15	12.05	6.13	0.92	3.00	102.0
8	7.40	12.05	6.13	1.47	3.00	119.0
9	17.00	12.05	6.13	3.01	3.00	170.0

Flow geometries and flow rates

All experiments were carried out on 50.8 mm diameter perspex tubing which allowed visualization of flow patterns, and the tubes were orientated for both vertical and horizontal flow. Nine different air–water flow rate combinations were used and the mixtures were produced by three different mixing devices. In two cases, air was injected through the wall into the flowing water either through a section of sintered bronze (referred to as the porous wall mixer), or a length of copper tube with 72 3.2 mm diameter holes in the wall (the drilled wall mixer). The third mixing device (the nozzle mixer) consisted of a cylindrical mixing chamber into which the water was injected through eight 12.7 mm diameter inlets located in the blank end of the mixer, with air injected through a 12.7 mm inlet in the centre of the water inlets. A conical reducing nozzle connected the mixing chamber to the test section. Further details of these devices may be obtained from the reference by Herringe (1973), and also Herringe & Davis (1976).

The nominal flow rates for the nine standard flow conditions are listed in table 1. The superficial gas velocity refers to the velocity which each phase would have if it alone flowed through the pipe and the values included in the table are based on the given mass flow rates with static pressure corresponding to the values 36 diameters downstream from the air–water mixers, with the pipe orientated vertically. These values give an indication of the relative volume flow rates of the two phases and show, for example, that flow conditions 3, 6 and 9 are relatively high void fraction flows. In fact these flows generally contained slugs of air, which are large, non-spherical bubbles of size approaching, or greater than the pipe dimension. In some cases these slugs could be observed through the pipe wall, while in others, the flows appeared will dispersed and the slugs could be detected only by inspection of the probe signals. A flow was designated as being a slug flow if the probe detected occassional bubbles which were an order of magnitude larger than the majority of detected bubbles.

Experiments into the flow structure were carried out at three axial locations: 8 diameters, 36 diameters and 108 diameters (8D, 36D and 108D) downstream from the mixing devices. Static pressure tappings were located at nine axial positions, up to the 108D locations.

EXPERIMENTAL RESULTS AND INTERPRETATION

At 8D, 36D and 108D, void profiles were obtained for both vertical and horizontal flows and typical results are presented in figure 1. With horizontal flow, stratification generally occurred, giving non-symmetrical void profiles with the majority of the gas in the top portion of the pipe. For some of these cases, void profiles were measured along a vertical and a horizontal diameter and results obtained were similar to those shown in figure 2.

The development of void profiles for vertical flow has been discussed in more detail by Herringe & Davis (1976). The results given in figure 1 show that the use of different types of

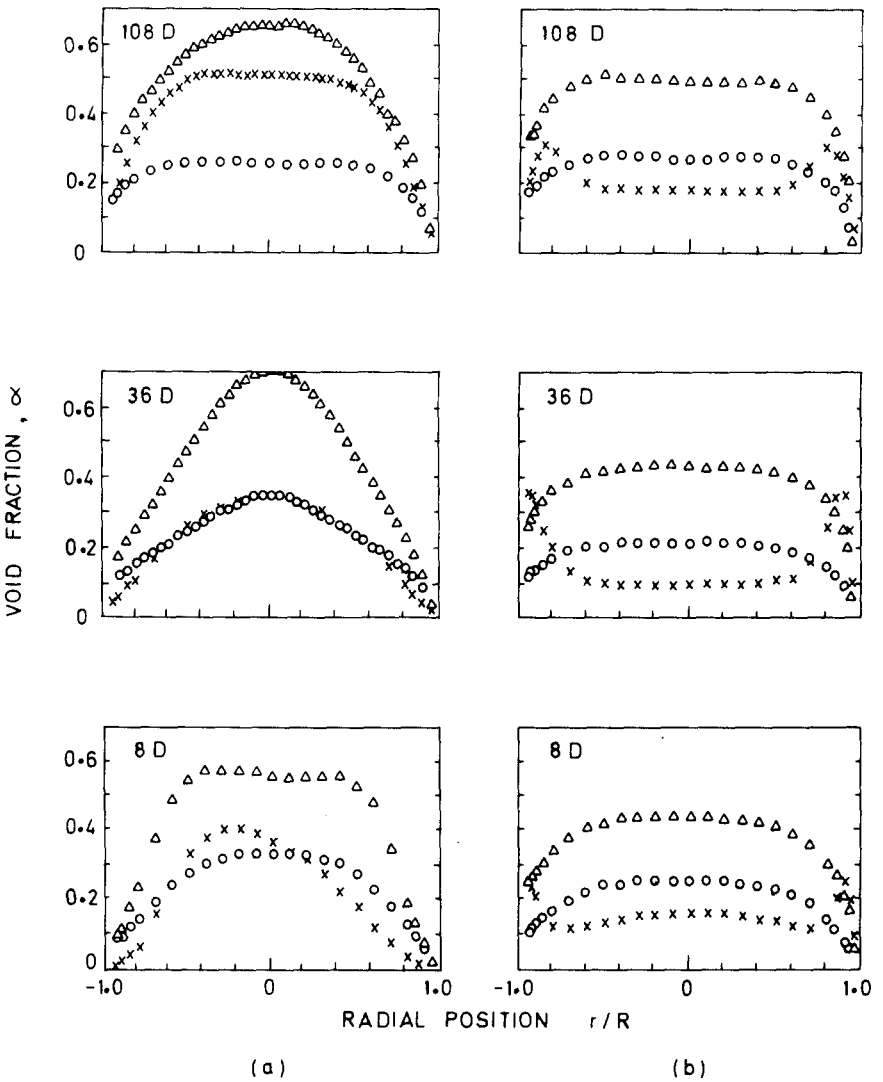

Figure 1. Voidage distributions in vertical upwards pipe flow. (a) Drilled wall mixer. (b) Multi-jet nozzle mixer. X - - - - Flow 2, $Fr = 11.6$, $\beta = 0.18$; Δ - - - - Flow 6, $Fr = 92$, $\beta = 0.36$; O - - - - Flow 8, $Fr = 121$, $\beta = 0.19$.

mixer produced flows initially quite different in their distribution of local mean void fraction. The drilled wall mixer generally give rise to flows which had a single maximum of voidage at the pipe center, and which showed a more varied profile development with sharper central maxima at the 36D position and a subsequent return to profiles with a flatter central portion. In contrast the nozzle mixer gave rise to profiles of voidage which showed relatively little change along the 108 diameter pipe length, with persistent local maxima near the wall at lower velocities and relatively uniform distributions of voidage at higher velocities. Other mixer configurations, including a porous wall of sintered bronze and all three types with the insertion of screens (60 mesh, 34 swg, 40.4% open area ratio) across the flow after the mixer gave rise to profiles which developed into forms similar to that shown in figure 1 for the nozzle mixer. It seems that the drilled wall mixer, with relatively large wall holes and much lower promotion of mixing, gave rise to distinctive profiles of voidage which did not develop as rapidly towards a condition independent of the mixing arrangement. (See also Herringe & Davis (1976) for further discussion of this aspect).

The horizontal flow void profiles in figure 2 indicate a more complex development of the internal flow structure, although in the majority of cases external visual observation of the flow

suggested that the mixtures were relatively homogeneous. This demonstrates a defect which is most likely present in flow classification schemes since these are usually based on visual observations and only the structure of the outermost regions of flow is noted. The internal stratification shown in figure 2 would probably not be detected and the flow would be represented on classification maps (for example Mandhane *et al.* (1974)) simply as a bubble or dispersed flow. In addition the spearation of phases for flow condition 6 was not detectable visually while large slugs of gas were indicated by the probe responses. Flow conditions 4 and 8 lie in bubble or dispersed flow regions of classification maps and flow condition 6 lies between the dispersed and slug flow regimes (see figure 9 and later discussion).

It is evident from the results shown in figure 2 that flows from the nozzle mixer all show a steady increase in the degree of stratification along the 108 diameters of pipe length, and that relatively low void fractions were present in the lower part of the pipe. As would be expected, this effect is relatively stronger at the lower flow velocity where turbulent mixing would be weaker. It is apparent from these results that lower mean flow kinetic energy is associated with weaker mixing and the development of internal stratification effects under horizontal conditions. The average Froude numbers for the flows were 51.0 (flow condition 4), 92 (condition 6) and 123 (condition 8), showing that the mean kinetic energy predominates over gravitational effects. However, the re-mixing of phases at right angles to the flow is influenced by the turbulent rather than the mean kinetic energy. As shown by Herringe & Davis (1976) a definite relation exists between turbulent kinetic energy and mean bubble size, which must be largely

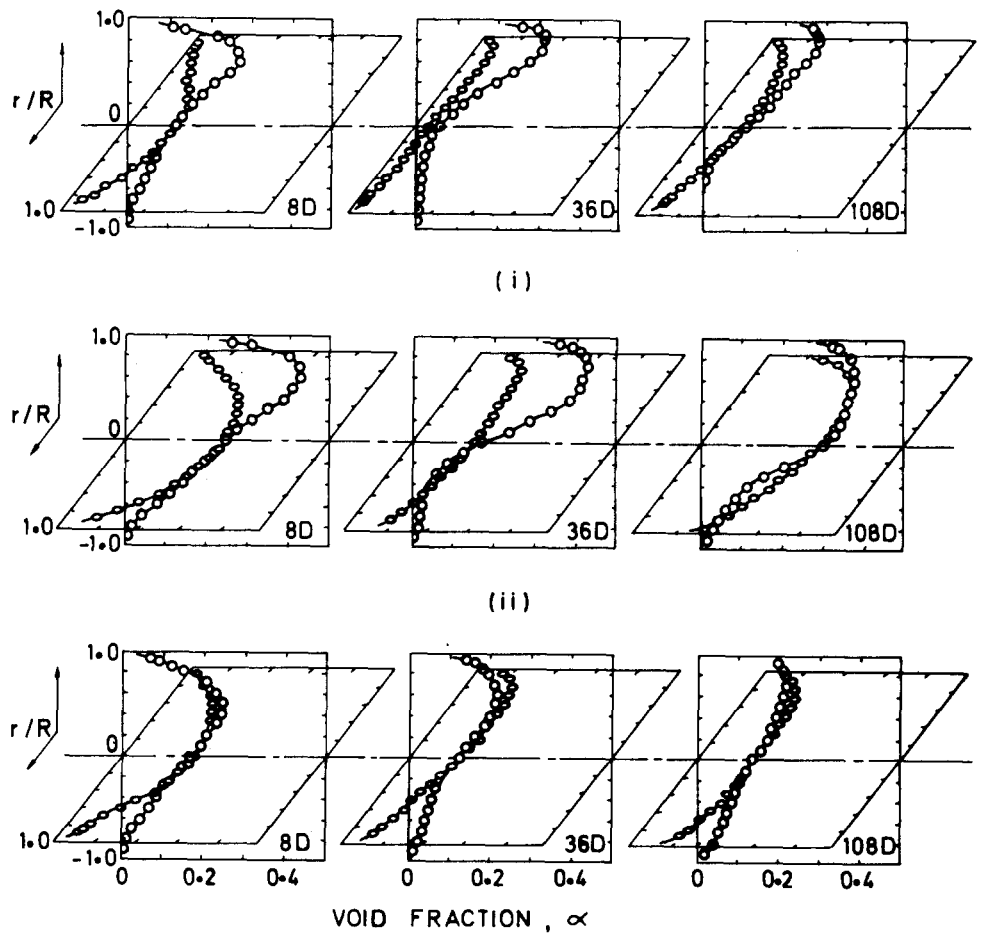

Fig. 2(a).

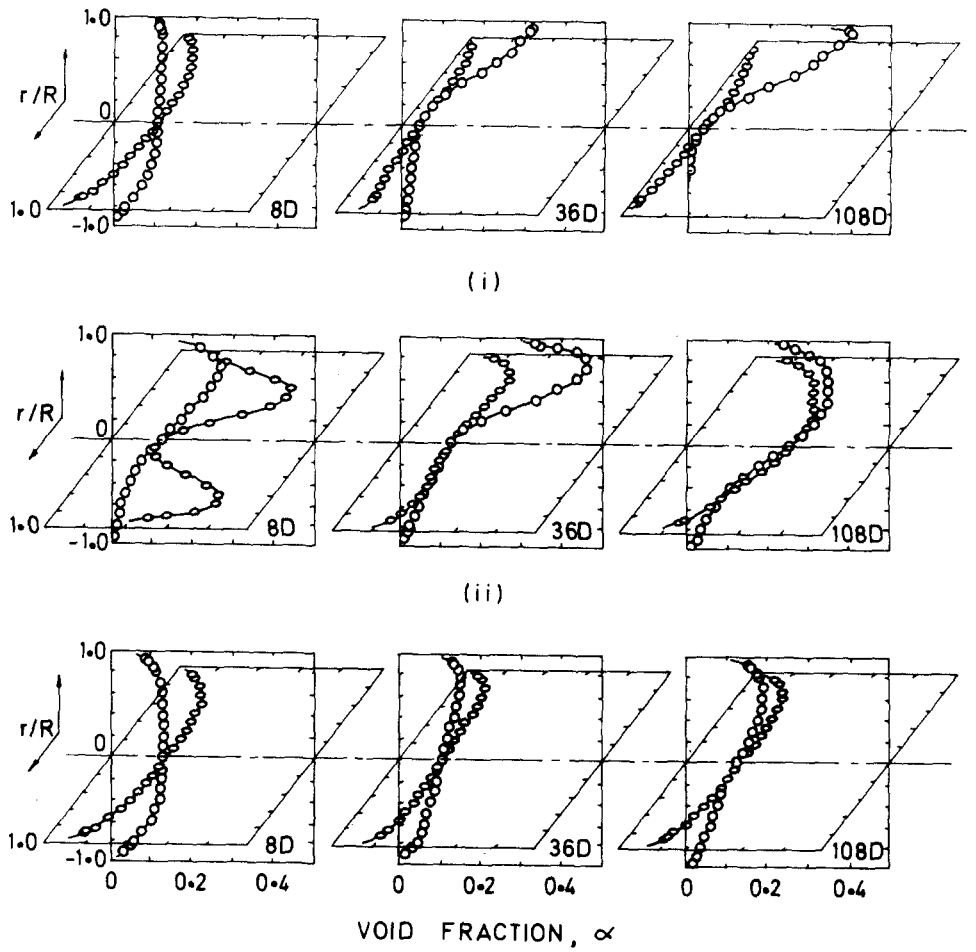

Fig. 2(b).

Figure 2. Voidage distributions in horizontal pipe flow. (a) Drilled wall mixer. (b) Multi-jet nozzle mixer. (i) Flow 4, $Fr = 51.0$, $\beta = 0.15$; (ii) Flow 6, $Fr = 92$, $\beta = 0.36$; (iii) Flow 8, $Fr = 121$, $\beta = 0.19$.

influenced by mixing effects at right angles to the flow direction. If turbulent velocities are of the order of 20% of the mean flow velocity as in single phase pipe flows (Laufer 1954), the Froude number based on turbulent kinetic energy would be smaller than the mixture Froude number by a factor of approximately 0.04. Thus it appears that the turbulent kinetic energy is likely to be in the range of two to 5 times the gravitational potential required to produce vertical transport within the pipe, and it is then physically reasonable that stratification should be observed and also that it is observed to be appreciably less at the highest velocity in the results shown in figure 2.

One interesting feature of the results of figure 2a was the production of maxima towards the walls by the nozzle mixer at the intermediate flow velocity (condition 6). It appears that this was a localized effect due to the mixer not apparent at other flow conditions and it was almost completely eliminated by mixing in the pipe by the 36 diameter position. It is likely that the apparent slight reduction of stratification between the 36 and 108D positions at this condition (flow 6), which was not observed at the higher or lower velocities, was associated with this unusual inlet void profile which may have facilitated stratification by virtue of the presence of regions of high gas concentration.

Flows from the drilled wall mixer (figure 2b) again show that the extent of stratification at the most distant position from the mixer is decreasing with the mean flow Froude number. Also, the trend for a steady slow increase of stratification along the pipe was observed for all flows.

This mixer did not give rise to the presence of two local maxima on the horizontal void profile, and generally produced flows which were substantially stratified close to the mixer whilst the nozzle mixer gave more homogeneous flow at this 8D downstream position. In this sense it appears that the drilled wall mixer produces in horizontal flow a void distribution more similar to that existing far downstream by virtue of the weaker mixing action, allowing the flow to stratify more rapidly. This in contrast to the vertical flow results, where it appeared that the nozzle mixer, with a stronger mixing action gave rise to flows which were initially more similar to those at positions far downstream.

More limited results at the lowest Froude numbers were obtained in horizontal flow conditions, with only the vertical void profiles being recorded. These results, in figure 3, show that the turbulent mixing of the nozzle mixer was then so weak that it also gave rise to flows which were initially stratified. At these low Froude numbers, the flow from both mixers showed a progressive development into distributions (at 108D from the mixer) which were flow rate dependent and not influenced by the mixer, with the lowest Froude number condition yielding the strongest stratification as expected. It was found that the flow from the porous wall mixer under horizontal flow conditions exhibited an initial stratification for all flow rates, and that flows from it were more similar to those from the drilled wall mixer. The nozzle mixer thus appears inappropriate for the modelling and study of horizontal flows as it does not give initial profiles of voidage similar to those which develop at large distances from the mixer, whilst the wall injection types do appear to give a more rapid development of stratification effects which inevitably develop under horizontal conditions. The wall injection mixers thus produce flows which represent more closely horizontal flows not influenced by particular mixer effects.

Velocity distributions for selected vertical flow experiments are shown in figure 4. It may be seen that these were generally quite similar in form for both types of mixer, except that at

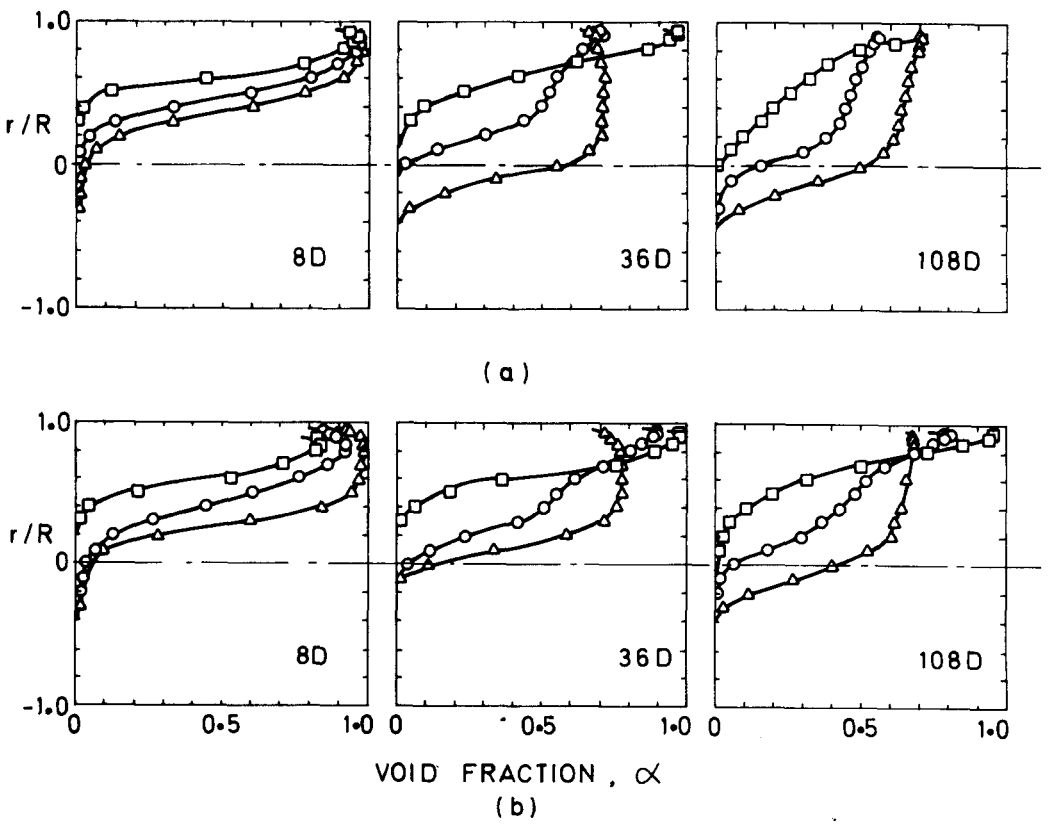

Figure 3. Voidage profiles across a vertical diameter in horizontal low velocity flow. (a) Drilled wall mixer. (b) Multi-jet nozzle mixer. □---- Flow 1, $Fr = 9$, $\beta = 0.087$; ○---- Flow 2, $Fr = 11.6$, $\beta = 0.18$; △---- Flow 3, $Fr = 17.5$, $\beta = 0.32$.

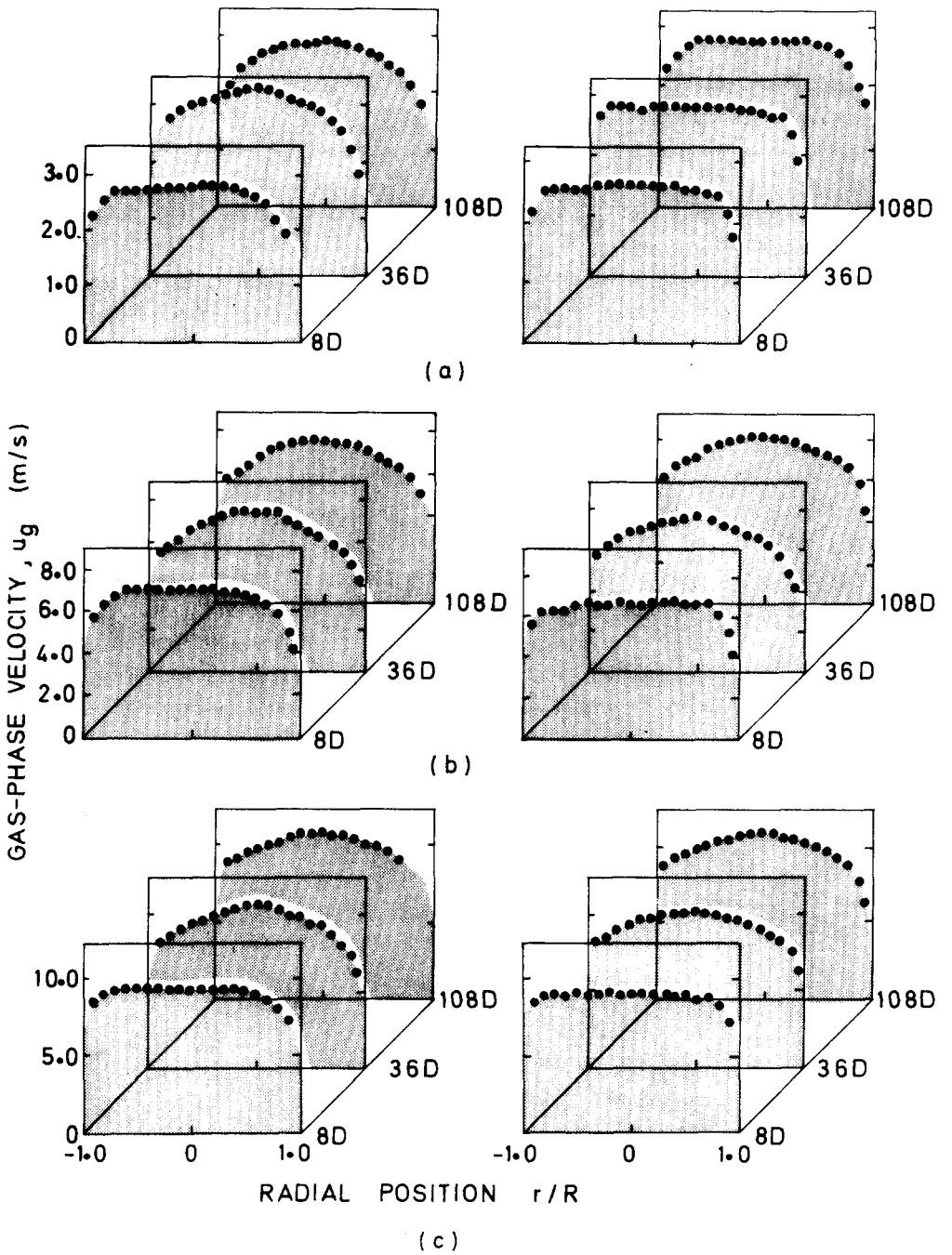

Figure 4. Velocity profiles in vertical upflow. (i) Drilled wall mixer. (ii) Multi-jet nozzle mixer. (a) Flow 2, $Fr = 11.6$, $\beta = 0.18$; (b) Flow 6, $Fr = 92$, $\beta = 0.86$; (c) Flow 9, $Fr = 121$, $\beta = 0.19$.

lower flow velocities the flow from the nozzle mixer maintains a somewhat flatter profile over the entire test length, whilst the flow from the drilled wall mixer shows evidence of a sharpening of the central maximum in the profile during the flow development. In view of the preceding discussion of the void profiles, it appears that this feature is associated with the development of the flow from this mixer which is evidently not mixer independent in vertical flows over the test length. A selection of velocity profiles for horizontal flow conditions is shown in figure 5. The results show that there is only a slight tendency for a higher velocity to develop in the region of high gas concentration in the upper part of the flow cross section (e.g. for flow condition 6 as shown) with this effect appearing negligible for the lower and higher

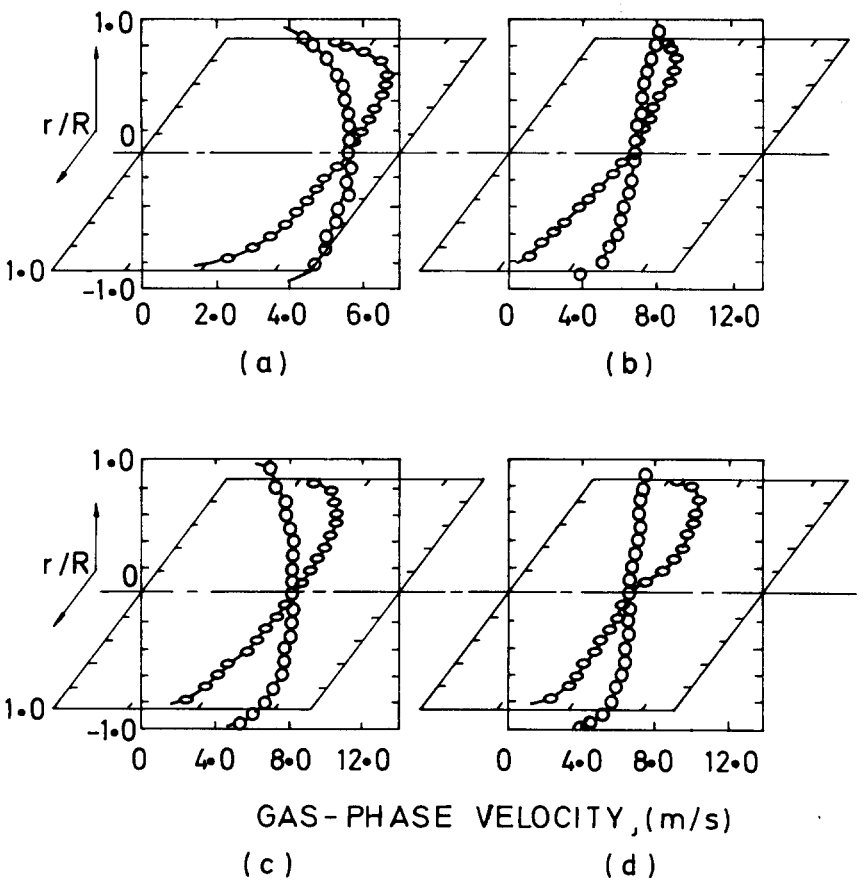

Figure 5. Velocity profiles in horizontal flow (36 diameters from mixer). (a) Porous wall mixer, Flow 4, $Fr = 51.0$, $\beta = 0.15$; (b) Porous wall mixer, Flow 6, $Fr = 92$, $\beta = 0.36$; (c) Porous wall mixer, Flow 8, $Fr = 121$, $\beta = 0.19$; (d) Nozzle mixer, Flow 6, $Fr = 92$, $\beta = 0.36$.

velocity conditions. Also it may be seen that the flow immediately downstream of the nozzle mixer in the condition where the void profile showed strong maxima away from the centre line (figure 2, flow condition 6) give rise to small but appreciable maxima in the velocity profiles away from the centre line. It appears however that this type of nozzle mixer, when used under conditions of horizontal flow, produces an initial flow which is appreciably different in nature to that which would develop far from the mixer. Again it seems that this highly turbulent form of mixing distorts the initial horizontal flow from that which ultimately tends to develop.

For selected flow conditions and axial locations, bubble diameter probability distributions were obtained at several radial positions, from which the mean detected bubble diameter was calculated. For vertical flows, these values were obtained at 8D and 108D to illustrate the flow development while for horizontal flow, representative results were taken at 36D. The probability distributions, as well as their interpretation, are presented and discussed in the reference by Herringe & Davis (1976) for vertical flows, where it was shown that the nozzle mixer in the vertical configuration also gave rise to initial bubble size distributions closest to those which exist at large distances from the mixer, whilst the drilled wall mixer gave initially appreciably larger bubbles in the central part of the pipe. It appears therefore that the conclusions reached above regarding the types of mixer which give flow structures most near those which persist far downstream (the nozzle in vertical flow and the drilled wall in horizontal flow) are reinforced by these studies of bubble size distribution. Summaries of mean bubble sizes at the centre line are given in table 3 and will be discussed later. It is clear that the turbulent action of the nozzle mixer results in substantially smaller bubbles.

FRICTIONAL PRESSURE GRADIENT

The friction factor can be calculated from [16] provided allowance is made for distribution effects which are completely defined by values of the velocity ratio, S and the momentum flux distribution parameter K. The velocity ratio allows determination of void fractions from measured volumetric flow rates

$$\langle\alpha\rangle = \beta/\{S(1-\beta)+\beta\}, \quad [38]$$

and the parameter K together with flow rate data allows determination of the dynamic head factor, D

$$D = K.(\langle\alpha\rangle\rho_G\bar{u}_G^2 + \langle 1-\alpha\rangle\rho_L\bar{u}_L^2)/p. \quad [39]$$

The experimental conditions for which the void and velocity profiles were measured allow determination of both S and K since β can be determined from flow rate measurements and the other area average quantities can be calculated by integrating over the pipe cross-section. When evaluating K, an additional assumption is required since values of liquid phase velocity have

Table 2. Velocity ratios, S and momentum flux distribution parameter K. K is in brackets ( )

Mixer	Flow condition	Vertical 8D	Vertical 36D	Vertical 108D	Horizontal 8D	Horizontal 36D	Horizontal 108D
	1	1.076	1.115	1.106			
Porous	2	1.038	1.051	1.069			
wall	3	1.046	1.164	1.189			
mixer	4	1.037	1.131	1.082	1.01	1.08 (1.021)	1.06
	5	1.024	1.116	1.080			
	6	0.982	1.031	1.159	1.37	1.49 (1.033)	1.05
	7	0.990	1.081	1.159			
	8	0.943	1.000	1.255	1.03	1.09 (1.018)	0.955
	9	0.887	0.991	1.262			
	1	1.336 (1.020)	1.227 (1.025)	1.299 (1.029)			
	2	1.136 (1.024)	1.123 (1.022)	1.006 (1.034)			
Drilled	3	1.237	1.273	1.146			
wall	4	1.000 (1.014)	1.225 (1.024)	1.122 (1.017)	1.00	1.12	1.00
mixer	5	0.992	1.007	1.068			
	6	0.914 (1.029)	1.152 (1.032)	1.121 (1.028)	1.11	1.34	1.00
	7	0.960	1.176	1.085			
	8	0.914	1.083	1.217	1.00	1.02	0.95
	9	0.876 (1.012)	1.136 (1.026)	1.285 (1.019)			
	1	1.000 (1.021)	1.084 (1.008)	1.179 (1.015)			
	2	1.000 (1.012)	1.028 (1.007)	1.031 (1.021)			
Nozzle	3	1.000	1.155	1.107			
mixer	4	1.046 (1.013)	1.117 (1.026)	1.071 (1.018)	1.14	1.01	1.06
	5	0.984	1.077	1.064			
	6	0.961 (1.016)	1.009 (1.026)	1.021 (1.017)	1.05 (1.017)	1.28	1.22
	7	1.021	1.161	1.092			
	8	0.941	1.127	1.060	1.04	1.10	1.13
	9	0.905 (1.008)	1.162 (1.017)	1.000 (1.018)			

not been measured. It was thus assumed that the *shape* of the liquid velocity profiles is the same as the shape of the gas velocity profiles. For horizontal flows where both vertical and horizontal profiles were measured, the area average quantities were calculated by assuming that the value of the quantity to be integrated was equal at any radial position to the average of the four measured values. The values of velocity ratio S and distribution parameter K calculated on this basis are given in table 2, where the numbers in brackets are the momentum flux distribution parameter, K.

The experiments into the flow structure were conducted at three axial locations (8, 36 and 108 diameters from mixer exit) while static pressures were recorded at nine axial positions Consequently average friction factors were determined over two separate lengths of flow; from 8D to 36D and from 36D to 108D; and over each length of pipe the average value of S and K was used. The assumption that terms T_1 and T_2 of [16] are negligible is shown to be realistic by the small changes in S and K over the more developed length from 36D to 108D. In all cases except vertical flow condition 9, T_2 is less than 1% of the pressure gradient (after subtracting the static head term) for the nozzle mixer, less than 1.1% for the drilled wall mixer and less than 2.1% for the porous wall mixer. The average percentage value of T_2 for all conditions was 0.7%. The term T_1 was evaluated where possible and was always less than 0.3% of the pressure gradient (minus the static head). For horizontal flows, it was not possible to evaluate T_1, although values of T_2 were generally less than 1% of the pressure gradient except for flow condition 6 which gave a value of T_2 approximately 3.5% of the pressure gradient for both wall injection type mixers.

The contribution of the two terms of [27] to errors in friction factor can be evaluated from knowledge of S and K, as well as the flow rate data. In all of the experiments, the product $\langle\alpha\rangle D$ was less than 0.072 so that the effect of an error in α is negligible (i.e. less than 0.078 $\mathrm{d}\langle\alpha\rangle/\langle\alpha\rangle$) and that any errors in f as calculated by the homogeneous flow model would be due to the second term of [27].

As shown in table 2, the distribution parameter K was not evaluated for all flows, although the velocity ratio was. Since there was not much variation in K, the average value of $K = 1.018$ has been used to calculate friction factors for the developed flow conditions. A comparison of

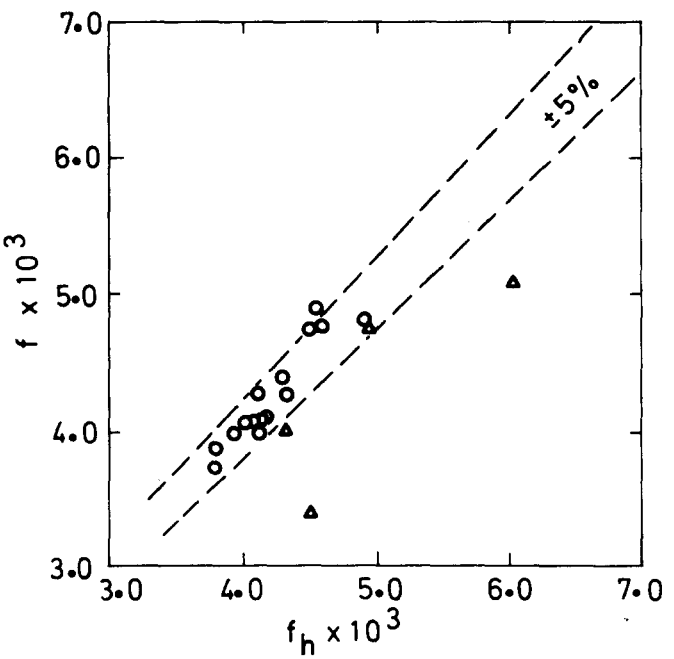

Fig. 6(a).

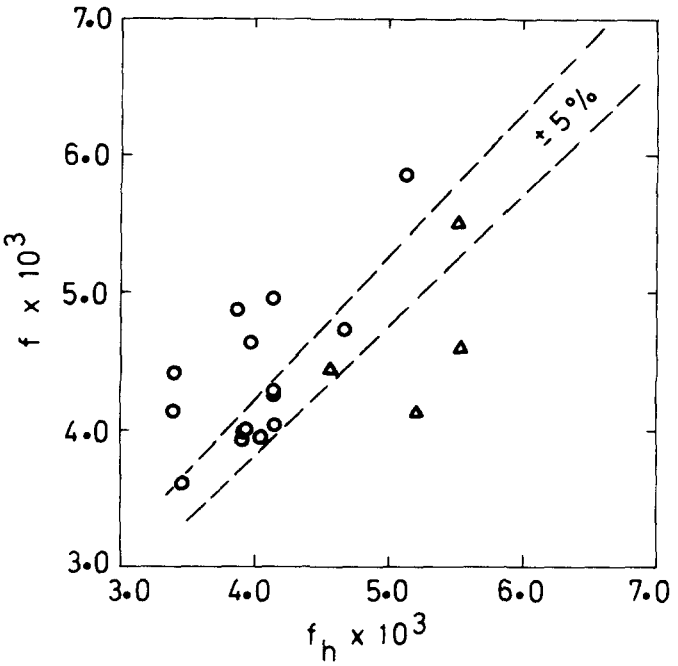

Fig. 6(b).

Figure 6. Comparison of friction factors obtained including distribution effects, f and based on homogeneous flow model, f_h. (a) Flow between 36 diameters and 108 diameters from mixers; (b) Flow between 8 diameters and 36 diameters from mixers; △ Frictional component less than 10% of pressure gradient.

friction factors based on the homogeneous model f_h, and calculated after allowing for distribution effects is given in figure 6. For the more developed region, from 36D to 108D, the difference in friction factor calculated by both methods is less than 5% except for those cases where the frictional component of the pressure gradient is less than 10%, or where slugging occurred. The complete results for flows from 36D to 108D are shown in figure 7, where they

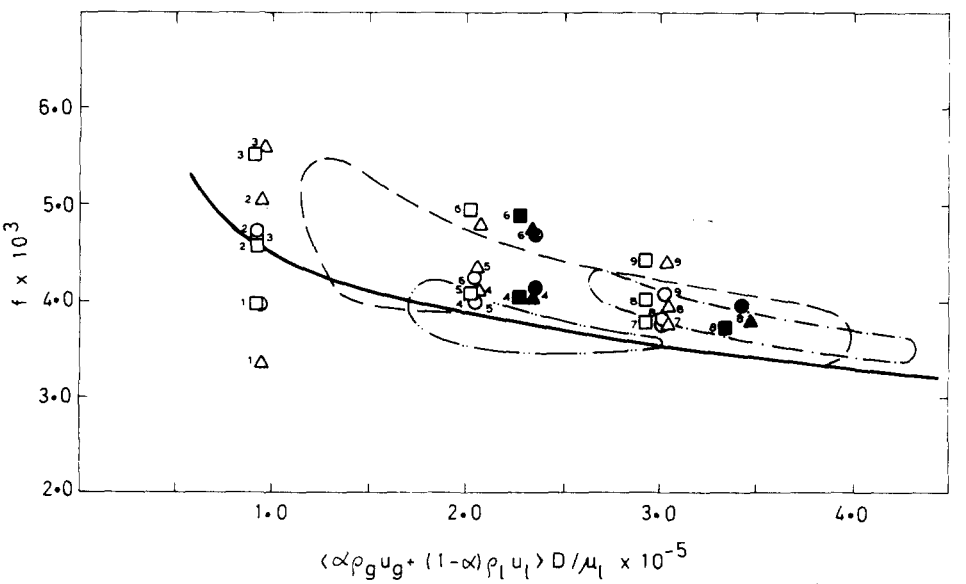

Figure 7. Friction factor–Reynolds number diagram for air/water mixtures. (Numbers denote flow conditions. Vertical upflow: open symbols. Horizontal flow: solid symbols). ▲, △ = Drilled wall mixer; ●, ○ Multi-jet nozzle mixer; ■, □ = Porous wall mixer (all between 36 diameters and 108 diameters from mixers); ——— = Nikuradse relation for single phase flow; – – – = Region of results of Davis (1974) for vertical and horizontal bubble flow (using a 38 mm pipe, $\alpha^* < 0.85$); — · — = Region of results of Kapalinsky & Bryant (1976) for horizontal flow (using a 50.4 mm pipe); — · · — = Region of results of Kopalinsky & Bryant (1976) for horizontal flow (using a 25.4 mm pipe).

are compared with single phase values. The high void fraction conditions (6 and 9) were observed (from resistivity probe responses) to give some internal slugs of gas in the flow from the wall injection type mixers, and as seen in figure 7 they gave relatively high friction factors. This is illustrated more clearly in figure 8 which shows the ratio of the two-phase friction factor (with allowance for phase distribution effects) to the single-phase friction factor f_w as a function of void fraction. The increase in the ratio with void fraction roughly follows the line

$$f/f_w = 1 + 0.22\langle\alpha\rangle + 0.82\langle\alpha\rangle^2.$$

Davis (1974) found that for high void fractions there was an apparent decrease in friction factor which it was suggested may have been due to phase separation, causing either slugging or errors in the momentum balance due to distribution effects. A comparison of the high void fraction results in figure 8 (for $\langle\alpha\rangle = 0.35$ and $\langle\alpha\rangle = 0.4$) shows that for the flows from the wall injection type mixers, which exhibited greater phase separation tendencies, the friction factors were higher than for the corresponding flows from the nozzle mixer. In fact, for a void fraction of 0.4 (flow condition 9), there was significant slugging in the flows from the wall injection mixers while no slugs were present in the flow from the nozzle mixer. Although the range of values of void fraction in figure 8 does not cover values as large as the range covered by Davis, the results do suggest that if phase separation (and/or slugging) did occur, then higher friction factors would result. The error in the value of D used in the homogeneous flow model can be estimated from the void and velocity profiles in the same way that K was evaluated. In general, $D_h < D$ with an average difference less than 1%, tending to decrease as $\langle\alpha\rangle$ increased, and actually becoming negative for $\langle\alpha\rangle \approx 0.4$ (i.e. $D_h > D$). This may lead to a negative error in homogeneous estimates of friction factor at higher void fractions. Further, the $d\langle\alpha\rangle/\langle\alpha\rangle$ term may become more significant at high $\langle\alpha\rangle$ and also contribute a negative error. This could explain the fall in homogeneous friction factor at high gas concentration in Davis' results as well as those reported by Kopalinsky and Bryant, but this can only be ascertained by having some means of estimating both $d\langle\alpha\rangle/\langle\alpha\rangle$ and dD/D for these flows.

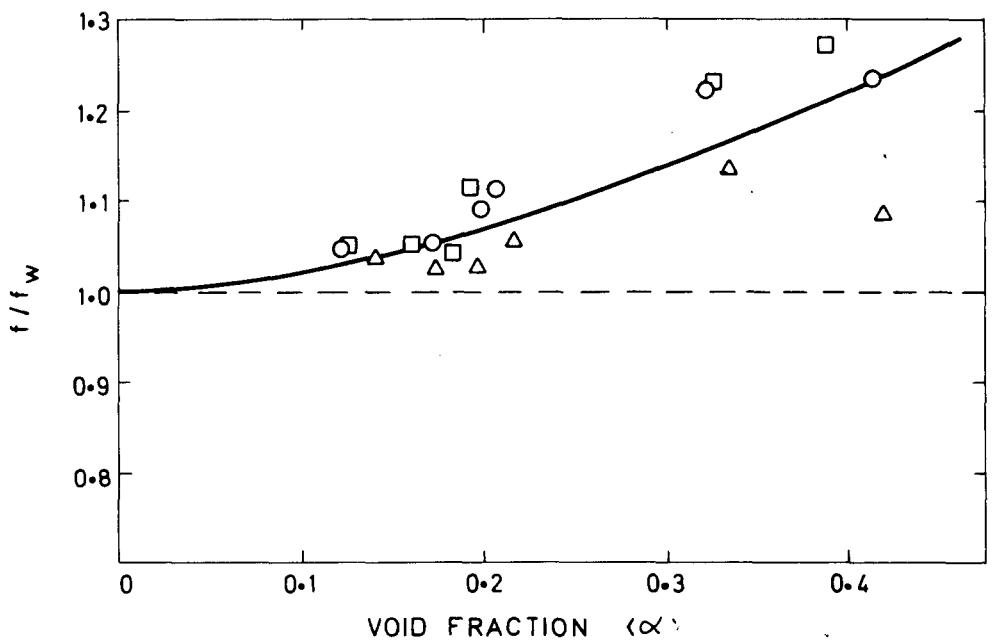

Figure 8. Divergence of two phase friction factors from single phase values as a function of void fraction. □ Porous wall mixer results; ○ Drilled wall mixer results; △ Nozzle mixer results. Solid line; fit to data. $f/f_w = 1 + 0.22\,\alpha + 0.82\,\alpha^2$.

DISCUSSION

As may be seen from figure 7, the dependence on pipe diameter appears quite significant in the earlier results, there being an apparent trend to higher friction factors with increasing pipe size for horizontal flows. This is consistent with the association of higher frictional effects with flows having relatively larger bubbles, as would result from the reduction of Froude number associated with an increase in pipe size. This effect becomes apparent again in the discussion of friction factors which follows.

The measurements of the flow structure demonstrate the need for ensuring that a flow is fully developed, or at "equilibrium" conditions, before results can be applied generally. The more detailed experiments into the vertical flow structure showed that different mixing devices produce flows of a different structure (represented by void profiles, velocity distributions and bubble size distribution). As the flows travel downstream, these differences diminished and by 108 diameters downstream, there was a convergence of flow patterns from the different mixers. This changing structure from the various mixers has an effect on the resulting pressure gradient as demonstrated by the results in Table 3. The changes in the mean detected bubble diameter at the centre of the pipe are shown together with the respective friction factors. In all cases in vertical flow (except flow conditions 1 and 2 from 8D to 36D) corresponding friction factors for flow from the drilled wall mixer were above the values for the nozzle mixer, whilst corresponding bubble sizes from the drilled wall mixer were above those from the nozzle. By 108D, the differences in bubble diameter from the two mixers appear insignificant (although flow condition 9 from the drilled wall mixer produced slugs which were not observed in the flow from the nozzle mixer). There is thus a consistency in these results and it appears that the higher friction factors for the drilled wall mixer reflect the greater resistance to shear and transmission of shear to the wall in flows having large bubble sizes. It may be seen that there is a general tendency for the friction factor to be higher in the developing region of the flow

Table 3. Relation between bubble growth and friction factors

Mixer type	Flow condition	Mean detected bubble diam. (mm) 8D	108D	Friction factor × 10^3 8D–36D	36D–108D
Drilled wall mixer (vertical flow)	1			0.415	0.339
	2	4.6	3.5	0.460	0.509
	3			0.750	0.562
	4	4.1	2.6	0.428	0.410
	5			0.446	0.433
	6	6.8	2.3	0.588	0.480
	7			0.433	0.377
	8			0.411	0.392
	9	4.6	2.6	0.497	0.440
Nozzle mixer (vertical flow)	1			0.444	0.400
	2	2.7	3.4	0.549	0.475
	3			0.327	0.468
	4	2.0	2.4	0.396	0.399
	5			0.373	0.400
	6	2.3	2.6	0.475	0.423
	7			0.402	0.375
	8			0.411	0.380
	9	1.9	2.5	0.465	0.408
Drilled wall mixer (horizontal flow at 36D)	4	4.4		0.363	0.402
	6	3.9		0.432	0.475
	8	4.1		0.384	0.380
Nozzle mixer (horizontal flow at 36D)	4	—		0.392	0.415
	6	—		0.479	0.474
	8	—		0.420	0.397

(between 8D and 36D) compared with that further downstream, this effect being greater for the drilled wall mixer which exhibits a stronger flow development due to its greater deviation from the ultimate equilibrium structure.

In horizontal flows the drilled wall mixer generally gave lower friction factors (i.e. the opposite effect to that in vertical flow). As a result of the difficulty of determining reliable distribution parameters from the asymmetric void distribution in horizontal flows, only a few values were determined. However, it does appear that the relative effects from the two types of mixer are reversed and that this behaviour is consistent with the observations of flow structure. That is, the nozzle mixer provides a flow structure which more closely approximates the flow at large distances from the mixer for vertical flows, whilst the drilled wall mixer gives flows which are more nearly mixer independent under horizontal flow conditions. In both vertical and horizontal flows it appears therefore that under conditions which are not strongly influenced by the mixer, a generally lower friction factor was observed. The results of table 3 also show that the mixer independent flow conditions in horizontal flow (i.e. from the drilled wall mixer) are associated with larger bubbles on the centre line than in vertical flow (i.e. from the nozzle mixer) although on the basis of the somewhat limited number of results it is difficult to form a general conclusion relating to bubble size for horizontal flows, especially in view of the strongly asymmetric void distributions.

Although the number of flow conditions discussed has been limited (9 flow rates for 3 different air–water mixers, for vertical and some horizontal flow), the combination of measurements of the flow structure with overall pressure loss measurements had yielded significant information.

For low Reynolds number flows ($Re < 10^5$) estimates of vertical flow friction factor are liable to be inaccurate because the frictional component represents only a small proportion ($< 10\%$ in the flows studied here) of the overall pressure gradient. This in itself significantly limits the accuracy of friction factor estimates, but it also means that distribution effects will be more significant than for higher Reynolds numbers. This undoubtedly contributes to the scatter in friction factors referred to by Wallis (1969) at low Reynolds numbers. Generally applicable frictional effects can only be accurately determined after a sufficient length has been allowed for flow development. From the experiments reported in this study a suggested minimum length is 108 diameter before mixer independent conditions are reached, but this is also dependent on the flow rates. Hence, because measurements were all taken within this length, the absolute values of friction factors reported in this work should be interpreted with caution. This, however, does not detract from the validity of the determination of the distribution and flow regime effects. The experimental results of Davis (1974) referred to earlier were based on pressure measurements between 24 and 100 diameters downstream from a mixing device similar to the nozzle mixer of this study. Similarly, the results of Kopalinsky & Bryant (1976) were for a nozzle mixer identical to that used in this study, with measurements up to 500 diameters from the nozzle. Although the flows studied by Davis were probably not fully developed, the results are shown by figure 7 to be consistent with Kopalinsky and Bryant. Similarly, the results of this study are in qualitative agreement, except for those flows containing gas slugs. It is clear from the present work, however, that before further detailed investigation of friction factor dependence on void fraction can be undertaken, flow structure and distribution effects must be taken into account.

The prediction from flow rates alone of whether a flow will contain slugs, and what the distribution effects will be, is not a simple matter. Many flow maps, indicating the occurrence of various flow regimes have been prepared and perhaps the most comprehensive are those proposed by Mandhane *et al.* (1974) for horizontal flows and by Oshinowo and Charles (1974) for vertical flows. The relevent portions of these flow pattern maps are presented in figure 9, together with the co-ordinates corresponding to the flow conditions of this study, 36 diameters from the mixers. As is evident from these diagrams, it is often not obvious what type of flow

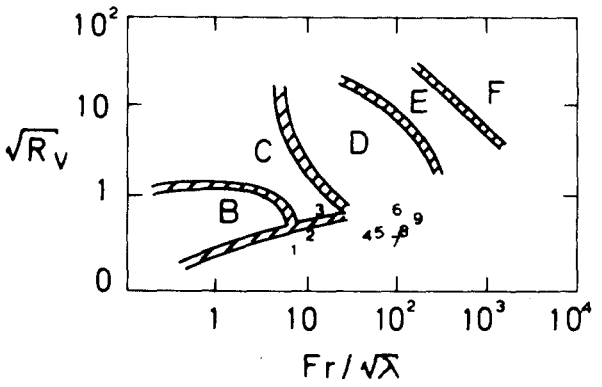

(a)

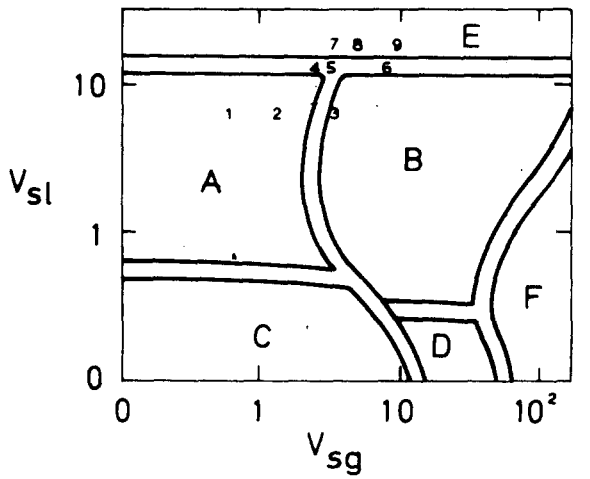

(b)

Figure 9. Flow conditions of present work located on flow pattern maps. (Numbers denote flow condition, table 1). (a) Vertical flow, from Oshinowo & Charles (1974). R_v = delivered gas to liquid volume ratio; $\lambda = 1$ for water.

Region	Flow mode
A	Bubble
B	Quiet slug
C	Dispersed slug
D	Frothy slug
E	Froth
F	Annular

(b) Horizontal flow, from Mandhane *et al.* (1974). V_{sL}, V_{sG} = superficial gas and liquid velocities.

Region	Flow mode
A	Bubble/elongated bubble
B	Slug
C	Stratified
D	Wave
E	Dispersed
F	Annular/mist

regime exists, partially because of the subjective way in which various regimes are defined. In general, it could be said that flows similar to conditions 4, 5, 7 and 8 of this study would be ones in which distribution effects can be safely neglected. These correspond to bubble and dispersed flows. Flow conditions 3 and 5 were definitely slug flows and in flow condition 9, the occurrence of slugs depended on the mixing device. The flow regime maps thus provide a general indication of the need to allow for regime effect. However, on the basis of the results reported in this study, it is not possible to make accurate general predictions on expected velocity ratios, especially where the flow has not passed along a sufficient length of pipe to be independent of upstream mixing effects. For developed flow conditions, a reasonable estimate of the momentum flux distribution parameter would be $K = 1.02$.

CONCLUSIONS

The one-dimensional equation of motion for the flow of a gas–liquid mixture along a pipe has been modified to correctly account for distribution effects. Provided phase and velocity distributions did not alter significantly along the pipe, the equation of motion could be integrated to relate the pressure distribution along the pipe to a friction factor and inlet flow conditions. The resulting equations were shown to be identical to those developed under the assumption of homogeneous flow, provided the correct definitions of void fraction and the dynamic head were used.

For bubbly, or dispersed gas–liquid pipe flows in which slugs of gas did not occur, friction factor estimates based on the homogeneous flow model were relatively unaffected by inclusion of concentration and velocity distributions. This suggests that trends reported in the literature, which show a dependence of friction factor on the relative gas to liquid flow rates are not solely the result of neglecting distribution effects in the momentum balance. For dispersed air–water flows, the most reliable estimates for the friction factor would be obtained by using the single phase value for 25 mm pipes, increased by 10% for 50 mm pipes, where the Reynolds number is defined on the basis of the liquid viscosity. In developing flow, and where slugs of gas occur further increases in friction would be expected.

For flows which had not reached mixer independent conditions, friction factors were relatively high. This was associated with the need to decrease the size of bubbles in the flow which were above their "equilibrium" size.

To simulate fully developed flow conditions, a highly turbulent mixer such as the multi-jet nozzle type is most suitable for vertical flows, while the low intensity type of mixer, such as the drilled wall type is more appropriate for horizontal flows.

REFERENCES

BEATTIE, D. R. H. 1972 Two-phase flow structure and mixing length theory. *Nucl. Engng Design* **21**, 46–64.

BEATTIE, D. R. H. 1973 A note on the calculation of two-phase pressure losses. *Nucl. Engng Design* **25**, 395–402.

DAVIS, M. R. 1974 The determination of wall friction for vertical and horizontal two-phase bubbly flows. *J. Fluid Engng* **96**, 173–179.

HERRINGE, R. A. 1973 A study of the structure of gas–liquid mixture flows. Ph.D. Thesis, University of New South Wales, Kensington, N.S.W., Australia.

HERRINGE, R. A. & DAVIS, M. R. 1974 Detection of Instantaneous phase changes in gas–liquid mixtures. *J. Phys. E.*, Scient. Instrum. **7**, 807–812.

HERRINGE, R. A. & DAVIS, M. R. 1976 Structural development of gas–liquid mixture flows. *J. Fluid Mech.* **73**, 97–123.

HUEY, C. T. & BRYANT, R. A. A. 1967 Isothermal homogeneous two-phase flow in horizontal pipes. *A.I.Ch.E. Jl.* **13**, 70–77.

KOPALINSKY, E. M. 1971 A study of bubbly two-phase flow. Ph.D. Thesis Univ of N.S.W., Australia.

KOPALINSKY, E. M. & BRYANT, R. A. A. 1976 Friction coefficients for bubbly-two-phase flow in horizontal pipes. *A.I.Ch.E. Jl.* **22**, 81–86.

LAUFER, J. 1954 The structure of turbulence in fully developed pipe flow. *N.A.C.A. Rep.* 1174.

MANDHANE, J. M., GREGORY, G. A. & AZIZ, K. 1974 A flow pattern map for gas–liquid flow in horizontal pipes, *Int. J. Multiphase Flow* **1**, 537–553.

OSHINOWO, T. & CHARLES, M. E. 1974 Vertical two-phase flows. Part 1. Flow pattern correlations. *Can. J. Chem. Engng* **52**, 25–34.

ROSE, S. C. & GRIFFITH, P. 1964 Report 5003–30, Massachusetts Institute of Technology.

TANGREN, R. F., DODGE, D. H. & SEIFERT, H. S. 1949 Compressibility effects in two-phase flow. *J. Appl. Phys.* **20**, 638–645.

WALLIS, G. B. 1969 *One-dimensional two-phase flow.* McGraw-Hill, New York.

ZUBER, N., STAUB, F. W., BIJWAARD, G. & KROEGER, P. G. 1967 Steady state and transient void fraction in two-phase flow systems, GEAP-5417.

APPENDIX

Equations of state

The density of the gas phase is related to initial conditions, denoted by suffix zero, by the equation

$$\rho_G = \rho_{G0}\bar{p}^{1/n}, \tag{A1}$$

where $\bar{p} = p/p_0$ = reduced dimensionless local pressure, n = polytropic index of gas phase.

The mixture density, defined as

$$\rho_m = \langle\alpha\rangle\rho_G + \langle 1-\alpha\rangle\rho_L$$

can thus be written

$$\rho_m = \langle\alpha\rangle\rho_{G0}\bar{p}^{1/n} + \langle 1-\alpha\rangle\rho_L. \tag{A2}$$

Using [9], [12], [13] of the main text and [A1], it can be shown that

$$\frac{\langle\alpha\rangle}{\langle\alpha_0\rangle} = \frac{\bar{P}^{-1/n}}{s/s_0\langle 1-\alpha_0\rangle + \langle\alpha_0\rangle\,\bar{P}^{-1/n}}, \tag{A3}$$

and

$$\frac{\rho_m}{\rho_{m_0}} = \frac{1}{s/s_0\langle 1-\alpha_0\rangle + \langle\alpha_0\rangle\bar{p}^{-1/n}} \cdot \frac{\langle\alpha_0\rangle\rho_{G0} + s/s_0\langle 1-\alpha_0\rangle\rho_L}{\langle\alpha_0\rangle\rho_{G0} + \langle 1-\alpha_0\rangle\rho_L}. \tag{A4}$$

Before the flow properties can be related to sonic point conditions, a relation is needed for the speed of sound in the mixture. The speed of sound through a compressible medium is defined by

$$a = \left(\frac{\partial p}{\partial \rho}\right)^{1/2}_{\text{isentropic}}, \tag{A5}$$

so that for the two-phase mixtures, this definition will be used where the mixture density will be as defined above. From [A4] it can be shown that

$$\left(\frac{\partial p}{\partial \rho_m}\right)^{1/2} = \left(\frac{np}{\alpha\rho_m}\right)^{1/2}.$$

The value of the compression index n to be used in calculating the speed of sound is that value which allows isentropic compression of the mixture, and will be denoted by n_i, so that

$$a = \left(\frac{n_i p}{\alpha \rho_m}\right)^{1/2}. \qquad [A6]$$

It should be noted at this stage that as α tends towards zero, a approaches infinity, and this relation [A6] becomes invalid. This is a direct result of the assumption that the liquid phase is incompressible.

To determine the value of n_i, compression of the mixture as a whole must be considered. If the mixture behaved as a gas, then the mixture compression would follow a polytropic law of the type

$$p/\rho_m{}^k = \text{constant}. \qquad [A7]$$

However, Tangren *et al.* (1949) showed that considering an energy balance of an isolated unit volume of the flowing mixture at any instant gives an equation of state of the form

$$p\left(\frac{1}{\rho_m} - \frac{1}{(1+\mu)\rho_L}\right)^{k'} = \text{constant}, \qquad [A8]$$

where μ is the ratio of the mass of gas to the mass of liquid contained in the volume and k' is defined by

$$k' = \frac{C_{pm}}{C_{vm}} = \frac{\mu C_p + C_L}{\mu C_v + C_L}, \qquad [A9]$$

where C_p, C_v are the constant pressure and constant volume specific heats of the gas phase, C_{pm} and C_{vm} corresponding values for the mixture and C_L is the specific heat of the liquid.

Equation [A8] can be expressed in the form

$$P\left(\frac{\alpha}{\rho_m}\right)^{k'} = \text{constant}, \qquad [A10]$$

and it is thus obvious that the mixture is not truly a quasi-perfect gas since [A8] is not the usual form of the compression law (that is, [A7]). It follows from [A10] that

$$P\left(\frac{\mu}{1+\mu} \cdot \frac{1}{\rho_G}\right)^{k'} = \text{constant}, \qquad [A11]$$

which, for a given two-phase mixture, becomes

$$P\left(\frac{1}{\rho_G}\right)^{k'} = \text{constant}. \qquad [A12]$$

Tangren *et al.* (1949) stated "that k' has a significance for adiabatic mixed flow similar to that of $\gamma (= C_p/C_v)$ in adiabatic gas flow". In fact k' is shown by [A12] to be the compression index of the gas phase consistent with adiabatic compression of the mixture. The value of n_i to be used in [A6] for the speed of sound of the mixture is thus

$$n_i = \frac{\mu C_p + C_L}{\mu C_v + C_L}, \qquad [A13]$$

and for most flow applications μ is very small so that n_i is approximately unity. Also, as μ tends to infinity, n_i approached C_p/C_v which is the adiabatic index of the gas phase alone, as would be expected with very small liquid content. It may be seen that the equations of state accurately represent the mixture as $\alpha \to 1$, provided the phases remain well mixed, since the compression characteristics of the gas phase are correctly represented. This is not the case as $\alpha \to 0$, since the liquid has been assumed incompressible and the prediction of the speed of sound in this limiting case is therefore erroneous.

If a constant R_m is defined in the same way as in the thermodynamics of gases by

$$R_m = C_{pm} - C_{vm}, \qquad \text{[A14]}$$

then the equation of state for the gas phase, with introduction of the mixture density definition can be rearranged to give, in terms of mixture properties,

$$\frac{P}{\rho_m} = \frac{R_m}{\alpha} T. \qquad \text{[A15]}$$

Here again, the mixture cannot be regarded as an ideal quasi-perfect gas since the equivalent gas constant in the mixture state equation (R_m/α), is void fraction dependent.

The above discussion indicates that whilst a ratio of specific heats may be defined for a two-phase gas–liquid mixture, the mixture does not follow a polytropic compression law of the same form as a perfect gas. Further, the definition of an equivalent gas constant for the mixture as the difference of the specific heats leads to a state equation of a form different from that for a perfect gas. It may be seen that the resulting equation of state [A15] and the polytropic law [A10] introduce a similar modified density term (ρ_m/α) when compared with the ideal gas relations, so that the mixture does not behave as a quasi-perfect gas. It has also been established that the specific heat ratio for the mixture is in fact equal to the compression index of the gas phase alone which allows isentropic compression of the mixture, and is approximately equal to one.